

EVIDENCE FOR BLUE STRAGGLER STARS REJUVENATING THE INTEGRATED SPECTRA OF GLOBULAR CLUSTERS

A. JAVIER CENARRO, J.L. CERVANTES, MICHAEL A. BEASLEY, ANTONIO MARÍN-FRANCH, ALEXANDRE VAZDEKIS
Instituto de Astrofísica de Canarias, Vía Láctea s/n, 38200 La Laguna, Tenerife, Spain

Draft version November 3, 2018

ABSTRACT

Integrated spectroscopy is the method of choice for deriving the ages of unresolved stellar systems. However, hot stellar evolutionary stages, such as hot horizontal branch stars and blue straggler stars (BSSs), can affect the integrated ages measured using Balmer lines. Such hot, “non-canonical” stars may lead to overestimations of the temperature of the main sequence turn-off, and therefore underestimations of the integrated age of a stellar population. Using an optimized $H\beta$ index in conjunction with HST/WFPC2 color-magnitude diagrams (CMDs), we show that Galactic globular clusters exhibit a large scatter in their apparent “spectroscopic” ages, which does not correspond to that in their CMD-derived ages. We find for the first time that the specific frequency of BSSs, defined within the same aperture as the integrated spectra, shows a clear correspondence with $H\beta$ in the sense that, at fixed metallicity, higher BSS ratios lead to younger *apparent* spectroscopic ages. Thus, the specific frequency of BSSs in globular clusters sets a fundamental limit on the accuracy for which spectroscopic ages can be determined for globular clusters, and maybe for other stellar systems like galaxies. The observational implications of this result are discussed.

Subject headings: blue stragglers — globular clusters: general — galaxies: star clusters — galaxies: stellar content

1. INTRODUCTION

A common method for estimating the ages of unresolved stellar systems is to measure Balmer lines and metal lines from integrated spectra, and compare them to stellar population models. The method relies on the fact that Balmer lines are mostly sensitive to the effective temperature (T_{eff}) of the main sequence (MS) turn-off of a stellar population (e.g. Buzzoni et al. 1994). This, in turn, provides a measure of the population age.

However, a longstanding concern over the use of Balmer lines to estimate spectroscopic ages is the effect of non-canonical evolutionary stages on the integrated stellar population spectra. Particularly worrisome are the possible effects that bluer horizontal branch (HB) stars and blue straggler stars (BSSs) may have on the inferred T_{eff} of the MS turn-off. HB stars are helium-burning stars which occupy a region in the CMD with a typical absolute V magnitude of ~ 0.7 mag (e.g. Harris 2001). BSSs are identified as blue, luminous extensions of MS stars (Sandage 1953). They are thought to form due to H refuelling processes after the MS stage, either from collisional stellar encounters (e.g. Davies et al. 1994) or from mass-transfer binaries (McCrea 1964). Both HB stars and BSSs with $T_{\text{eff}} > 6500$ K show prominent Balmer lines in their spectra, which can mimic the presence of younger stellar populations (e.g. Rose 1985, Lee et al. 2000, Schiavon et al. 2004; Trager et al. 2005).

In a recent paper, Cervantes & Vazdekis (2008) defined an optimized line-strength index for $H\beta$, called $H\beta_o$, that minimizes the metallicity dependence of the Balmer line in favor of its age sensitivity. Interestingly, as pointed out in that paper, the integrated spectra of Galactic globular clusters (GGCs) from Schiavon et al. (2005; hereafter S05) exhibit a clear intrinsic scatter in their $H\beta_o$

strengths, particularly with increasing metallicity.

In order to shed light on the above issue, in this *letter* we combine resolved and unresolved data of such GGCs to investigate whether CMD-based age differences among GGCs and/or different relative contributions of non-canonical stages can be responsible for the distinct integrated $H\beta_o$ indices. In Section 2 we discuss the data used in this study, the analysis of which is described in Section 3. Finally, in Section 4 we present our conclusions and discuss our findings within the context of estimating ages for unresolved stellar populations.

2. THE DATA

Integrated optical spectra for 41 GGCs were taken from S05. These data were obtained by drift-scanning the core diameter of each GGC –with a spectroscopic aperture equal to this diameter– in order to construct a representative integrated spectrum. The spectra cover a wavelength range of $\sim 3350 - 6430\text{\AA}$ with a FWHM of $\sim 3.1\text{\AA}$ and typical signal-to-noise ratios (S/N) of $\sim 250\text{\AA}^{-1}$ in the continuum of the $H\beta$ line. We refer the reader to S05 for more details on these data.

In Figure 1 we present the indices $H\beta_o$, $H\beta_{\text{LICK}}$ (Worthey et al. 1994) and $[\text{MgFe}]$ (González 1993) measured for the 41 GGC spectra at the S05 spectral resolution. Uncertainties in the index measurements (1σ error bars) account for the S/N spectra and the typical radial velocity error provided by S05 for each GGC. To guide the eye, based on the MILES stellar library (Sánchez-Blázquez et al. 2006a; Cenarro et al. 2007a), an extension of the simple stellar population (SSP) models in Vazdekis (1999) are overplotted at 3.1\AA spectral resolution (hereafter V99+). The fact that most GGCs lie below the model grids arises from the well-known zero-point problem of SSP models (e.g. Vazdekis et al. 2001; Schiavon et al. 2002), although this does not affect our results which

are based on relative differences.

As expected, in the $H\beta_o$ plot (Fig. 1a) GGCs follow – on average – an old sequence in metallicity. However, by simple visual inspection they seem to separate into two groups, particularly at the high metallicity end ($[MgFe] \gtrsim 1.2$). Hence, solid and open symbols are employed to indicate, respectively, GGCs with *high* and *low* $H\beta_o$ values at fixed $[MgFe]$. Henceforth, these are referred to as *GGCH* and *GGCL* respectively.

When using the $H\beta_{LICK}$ definition (Fig. 1b), both GGC groups are still distinguished, although the greater age–metallicity degeneracy of $H\beta_{LICK}$ would make their differentiation less clear to detect if the distinct symbol codes were not present. Even so, Puzia et al. (2002) already pointed out the existence of unexpected $H\beta_{LICK}$ differences among certain metal rich (MR) GGCs. It therefore appears that some property differs between both groups leading to different Balmer-line strengths at a given metallicity. In fact, since the effect seems to increase with the increasing metallicity, we focus our analysis on those 25 GGCs from S05 with $[Fe/H] > -1.35$ ($[MgFe] \gtrsim 1.2$) among which clear differences in $H\beta$ at fixed metallicity are observed.

Together with the indices in Fig. 1, the adopted CMD-derived parameters for the 25 GGCs are listed in Table 1. The HB morphology, as measured by the HBR parameter (Lee et al. 1994), and the specific frequency of RR Lyrae variables, $S_{RRLyrae}$, are taken from the Harris (1996) catalogue (Feb 2003 revision; hereafter H03). We adopted the relative age estimates from De Angeli et al. (2005) and Recio-Blanco et al. (2006), whose applied the so-called vertical method on the GGC HST/WFPC2 snapshot catalogue of Piotto et al. (2002). Also based on that catalogue, Recio-Blanco et al. (2006) estimated the maximum T_{eff} along the HB, $T_{eff,HB}$ –considered as an HB morphology parameter–, whereas Moretti et al. (2008; hereafter M08) measured the logarithm of the number of BSSs inside the core radius, r_c , normalised to the sampled luminosity –in units of $10^4 L_\odot$ – in the $F555W$ HST band within the same aperture. The last quantity can be considered as a logarithmic specific frequency of BSSs inside the GGC r_c , hereafter $S_{BSS}^{r_c}$, and is representative of the spectroscopic data in S05 as they are both computed within the same aperture.

3. ANALYSIS

With the aim of constraining the origin of the intrinsic scatter in the Balmer line-strengths of our GGC subsample, in Figure 2 we show the CMD-derived parameters of Section 2 –where available– as a function of the GGC metallicity from H03. Symbol codes are kept as in Fig 1 except for the MR *GGCHs* NGC6388 and NGC6441, which being well-known *second parameter* clusters (Rich et al. 1997), are plotted as open stars –rather than solid squares– to facilitate further discussion.

In Fig. 2a, we see that there is no dependence of the group location on the CMD-derived age. The difference in $H\beta$ strengths between both groups is therefore not due to age differences among the GGCs, as would normally be inferred from a classical SSP index-index analysis. Note also that the typical dispersion of ~ 1 Gyr quoted by De Angeli et al. (2005) among the CMD-derived ages of intermediate metallicity GGCs could never explain the large scatter in $H\beta$. We also rule out the possibility that

the number of RR lyraes in the instability strip is playing a significant role, as the two GGC groups are well mixed (Fig. 2b). In addition we find that there is no obvious dependence on the HB morphology, as measured by either the HBR parameter or the maximum T_{eff} of the HB (Fig. 2c and Fig. 2d, respectively). As expected, the second parameter clusters NGC6388 and NGC6441 (open stars) do stand out of the general trends in both panels. Their high $H\beta$ strengths are naturally explained by the addition of hot HB stars in their integrated spectra.

Besides basic properties of the GGC CMDs, literature estimates of $[\alpha/Fe]$ for the GGCs in S05 (where available) show a high degree of homogeneity (e.g. Pritzl et al. 2005), so differing levels of α -elements cannot account for the observed differences. We have also ruled out that the Balmer lines of *GGCLs* are systematically filled-in by emission. In fact, emission was found and corrected by S05 for only NGC6171 and NGC6553 (*GGCHs*), and NGC6352 (*GGCL*). Interestingly, the fact that NGC6352 has the weakest $H\beta$ line of the sample may suggest that a residual emission could still be present.

Having rejected the above mechanisms from being responsible for the observed differences in $H\beta$ between *GGCHs* and *GGCLs* –except in the obvious case of NGC6388 and NGC6441–, in Fig 2e we show the GGC metallicities versus $S_{BSS}^{r_c}$. Interestingly, *GGCHs* and *GGCLs* –which were identified spectroscopically– separate cleanly into two groups in terms of their BSS specific frequencies. At a given metallicity, GGCs with higher $S_{BSS}^{r_c}$ values exhibit stronger $H\beta$ lines, suggesting that BSSs are indeed affecting their integrated spectra.

To reinforce this result, we quantify the impact of BSSs on the integrated spectrum of NGC6342, the *GGCH* with the highest $S_{BSS}^{r_c}$. Based on photometric data from H03 and M08 for this GGC and its BSS population, we obtain that 13% of the GGC flux in V band within r_c comes from a population of 7 BSSs with $0.22 \leq B - V \leq 0.52$, and a luminosity-weighted $B - V$ of 0.33. For each BSS, assuming $[Fe/H] = -0.65$ and its $B - V$, we estimate T_{eff} using the $(B - V) - T_{eff}$ relation for dwarfs from Alonso et al. (1996). The T_{eff} values of the 7 BSSs are in the range $5925 \leq T_{eff} \leq 7500$ K. We then compute spectral BSS templates with the above parameters on the basis of the MILES stellar library, using the interpolating algorithm in Vazdekis et al. (2003; Appendix B). After the 7 BSS templates are scaled according to their V fluxes and subtracted from the NGC6342 spectrum, its integrated $H\beta_o$ and $H\beta_{LICK}$ indices decrease by 0.70 \AA and 0.62 \AA respectively. Taking into account that the averaged $S_{BSS}^{r_c}$ of *GGCLs* with $[Fe/H] > -0.8$ (similar to that of NGC6342) is ~ 1.4 (Fig. 2e), and assuming similar T_{eff} values for their BSS populations, the relative offsets in $H\beta_o$ and $H\beta_{LICK}$ between NGC6342 and the above *GGCLs* are, respectively, 0.58 \AA and 0.51 \AA . This agrees with the differences between *GGCHs* and *GGCLs* obtained at this metallicity regime ($[MgFe] \gtrsim 2$; Fig. 1), supporting the idea that BSSs are responsible for the observed differences in $H\beta$. Even more, the effect of BSSs is also detected among the subsample of *GGCLs* with $[Fe/H] > -0.8$. NGC0104 and NGC6624, with extreme values of $S_{BSS}^{r_c}$, pose the lowest and largest $H\beta_o$ values respectively.

4. DISCUSSION

Based on the close correspondence between the specific frequency of BSSs in GGCs with $[\text{Fe}/\text{H}] > -1.35$ and their integrated $\text{H}\beta$ strengths at fixed metallicity, we conclude that BSSs are primarily responsible for the $\text{H}\beta$ variations observed in the integrated spectra of GGCs of intermediate-to-high metallicity. Far from discussing on the origin for the distinct $S_{\text{BSS}}^{r_c}$ values among GGCs (see M08 for a thorough study on this topic), we here analyze the implications of the above result in the context of age-dating unresolved stellar populations.

First, caution must be employed in Balmer-line based age-metallicity studies of unresolved extragalactic globular clusters (EGCs). Cenarro et al. (2007b) already reported the existence of EGCs with strong Balmer lines that were consistent with hosting an additional population of either blue HB stars and/or BSSs. Since the BSS fraction of EGCs is generally not known, the finding in this letter sets a fundamental limit to the reliability with which ages may be determined for EGCs using Balmer lines and SSP models. Taking the S05 data as a representative old GC system, we can estimate this limit from the averaged offsets in the measured $\text{H}\beta$ lines of GGCHs and GGCLs. Since the offsets seem to vary with metallicity, local linear fits to all GGCHs and GGCLs in Fig. 1 with $[\text{MgFe}] > 1.5$ ($[\text{Fe}/\text{H}] \gtrsim -1.0$) have been performed. For instance, at the location of 47Tuc (NGC0104; $[\text{MgFe}] \sim 2.31$), we obtain $\Delta\text{H}\beta_0 = 0.46 \pm 0.03 \text{ \AA}$ and $\Delta\text{H}\beta_{\text{LICK}} = 0.33 \pm 0.04 \text{ \AA}$ (at the S05 resolution) with uncertainties accounting for the standard errors of the means. Thus, assuming that GGCLs are ~ 14 Gyr old –the largest SSP age in Fig. 1– the two offsets can be consistently misinterpreted on the basis of SSP models as GGCHs being $\sim 6 - 7$ Gyr old, that is, as a rejuvenation of up to ~ 8 Gyr. Differences between GGCHs and GGCLs also exist for the Lick $\text{H}\gamma$ and $\text{H}\delta$ indices (Worthey & Ottaviani 1997), although they are not so apparent, probably due to their limited age-disentangling power for old SSPs. For these indices, the above test leads to rejuvenations of up to $\sim 4 - 5$ Gyr.

The role of metallicity in the present discussion is worthwhile considering. Although the relation between $S_{\text{BSS}}^{r_c}$ and metallicity is not statistically significant – but marginally positive – over the entire GGC sample (in agreement with M08), we find clear correlations for GGCHs and GGCLs separately, as illustrated by the solid lines in Fig. 2e. The different slopes seem to indicate that, when BSSs are important, their relative contributions are larger at high metallicities. Note that the fading with metallicity expected in $F555W$ band for the

most MR GGCs only accounts for up to $\Delta S_{\text{BSS}}^{r_c} \sim 0.2$, so the above trends are irrespective of this effect.

These results may also have important consequences for EGC studies. To understand the origin of color bimodality in GC systems within a context of galaxy formation, age-dating GC subpopulations –through the analysis of their integrated Balmer lines– is a common practice (see Brodie & Strader 2006 and references therein). Interestingly, some papers have reported that the MR GC subpopulation of certain galaxies show on average a smaller mean age and a larger age scatter than their metal poor (MP) counterparts (e.g. Puzia et al. 2005). Although the present finding does not rule out the existence of *true* age differences between MP and MR GC subpopulations, the increasing importance of BSSs with metallicity might, at least, partially affect the results of previous work.

Whether all the above results can compromise the integrated ages of other stellar systems, like galaxies, may rely on the mechanism that dominates the formation of BSSs. If stellar encounters were driving the BSS population, then one should not expect a major effect in galaxies because of their much lower stellar densities. However, this would not apply if mass-transfer binaries were the progenitors of most BSSs. In fact, Momany et al. (2007) and Mapelli et al. (2007) support the last scenario to explain the large BSS populations of dwarf spheroidal galaxies, and Han et al. (2007) have demonstrated the importance of binary interactions to understand the UV-upturn of elliptical galaxies (Es). It therefore seems that BSSs could play a non-negligible role in the integrated spectra of galaxies as long as they host an important fraction of binary stars. If this were the case and the potential increasing importance of BSSs with metallicity would still hold for massive Es, then BSSs could contribute to the age scatter reported for massive Es and to the fact that *younger* Es have higher metallicities than *older* Es (e.g. Trager et al. 2000; Sánchez-Blázquez et al. 2006b). This picture, however, requires of further investigation which is out of the scope of this paper.

We acknowledge the anonymous referee for very useful comments. A.J.C. and A.M-F are Juan de la Cierva Fellows of the Spanish Ministry of Education and Science (SMES). JLC acknowledges the SMES for a FPU PhD fellowship. This work has been funded by the SMES through grant AYA2007-67752-C03-01.

REFERENCES

- Alonso, A., Arribas, S., & Martínez-Roger, C. 1996, *A&A*, 313, 873
 Brodie, J. P., & Strader, J. 2006, *ARA&A*, 44, 193
 Buzzoni, A., Mantegazza, L., & Gariboldi, G. 1994, *AJ*, 107, 513
 Cenarro, A. J., Peletier, R. F., Sánchez-Blázquez, P., Selam, S. O., Toloba, E., Cardiel, N., Falcón-Barroso, J., Gorgas, J., Jiménez-Vicente, J., & Vazdekis, A. 2007a, *MNRAS*, 374, 664
 Cenarro, A. J., Beasley, M. A., Strader, J., Brodie, J. P., & Forbes, D. A. 2007b, *AJ*, 134, 391
 Cervantes, J. L., & Vazdekis, A. 2008, *MNRAS*, in press (arXiv:0810.3240)
 Davies, M. B., Benz, W., & Hills, J. G. 1994, *ApJ*, 424, 870
 De Angeli, F., Piotto, G., Cassisi, S., Busso, G., Recio-Blanco, A., Salaris, M., Aparicio, A., & Rosenberg, A. 2005, *AJ*, 130, 116.
 González, J. J., 1993, PhDT, University of California
 Han, Z., Podsiadlowski, Ph., & Lynas-Gray, A. E. 2007, *MNRAS*, 380, 1098
 Harris, W. E., 1996, *AJ*, 112, 1487
 Harris, W. E. 2001, in *Star Clusters*, ed. L. Labhardt & Binggeli (Berlin: Springer), 223
 Lee, Y., Demarque, P., & Zinn, R. 1994, *ApJ*, 423, 248
 Lee, H., Yoon, S., & Lee, Y. 2000, *AJ*, 120, 998
 Mapelli, M., Ripamonti, E., Tolstoy, E., Sigurdsson, S., Irwin, M. J., & Battaglia, G. 2007, *MNRAS*, 380, 1127
 McCrea, W. H. 1964, *MNRAS*, 128, 147
 Momany, Y., Held, E. V., Saviane, I., Zaggia, S., Rizzi, L., & Gullieuszik, M. 2007, *A&A*, 468, 973
 Moretti, A., De Angeli, F., & Piotto, G. 2008, *A&A*, 483, 183 (M08)
 Piotto et al., 2002, *A&A*, 391, 945
 Pritzl, B. J., Venn, K. A., & Irwin, M. 2005, *AJ*, 130, 2140

TABLE 1
 GALACTIC GLOBULAR CLUSTERS IN SCHIAVON ET AL. (2005) WITH $[\text{Fe}/\text{H}] > -1.35$

| GGC | Group ^a | $H\beta_o$ ^b | $H\beta_{\text{LICK}}$ ^b | $[\text{MgFe}]^b$ | $[\text{Fe}/\text{H}]^c$ | A_{GENORM}^d | S_{RRLYR}^c | HBR ^c | $\log(T_{\text{eff}} \text{ HB})^e$ | $S_{\text{BSS}}^{r,c,f}$ |
|---------|--------------------|-------------------------|-------------------------------------|-------------------|--------------------------|-----------------------|----------------------|--------------------|-------------------------------------|--------------------------|
| NGC0104 | L | 2.30 ± 0.02 | 1.55 ± 0.01 | 2.31 ± 0.02 | -0.76 | 0.99 | 0.2 | -0.99 | 3.756 | 1.03 |
| NGC1851 | H | 2.99 ± 0.03 | 2.27 ± 0.02 | 1.32 ± 0.02 | -1.22 | 0.81 | 13.5 | -0.36 | 4.097 | 1.48 |
| NGC2808 | L | 2.69 ± 0.01 | 2.01 ± 0.01 | 1.32 ± 0.02 | -1.15 | 0.76 | 0.3 | -0.49 | 4.568 | 0.94 |
| NGC5904 | H | 3.06 ± 0.01 | 2.42 ± 0.01 | 1.18 ± 0.01 | -1.27 | 0.81 | 37.7 | +0.31 | 4.176 | 1.07 |
| NGC5927 | L | 2.43 ± 0.03 | 1.38 ± 0.03 | 2.87 ± 0.02 | -0.37 | 0.92 | 0.0 | -1.00 | 3.724 | 1.40 |
| NGC6121 | H | 3.12 ± 0.03 | 2.28 ± 0.03 | 1.34 ± 0.02 | -1.20 | 0.91 | 52.7 | -0.06 | — | — |
| NGC6171 | H | 2.81 ± 0.05 | 2.08 ± 0.05 | 1.76 ± 0.03 | -1.04 | 0.99 | 31.0 | -0.73 | 3.875 | 1.68 |
| NGC6266 | H | 2.88 ± 0.02 | 2.09 ± 0.02 | 1.41 ± 0.02 | -1.29 | 0.92 | 15.6 | +0.32 | 4.477 | 0.96 |
| NGC6284 | H | 3.13 ± 0.04 | 2.33 ± 0.04 | 1.31 ± 0.03 | -1.32 | 0.87 | 3.9 | — | 4.279 | 0.97 |
| NGC6304 | L | 2.41 ± 0.05 | 1.47 ± 0.04 | 2.63 ± 0.03 | -0.59 | — | 0.0 | -1.00 | 3.724 | 1.51 |
| NGC6316 | L | 2.47 ± 0.04 | 1.46 ± 0.04 | 2.13 ± 0.02 | -0.55 | — | — | -1.00 | — | — |
| NGC6342 | H | 2.92 ± 0.11 | 2.07 ± 0.09 | 2.00 ± 0.06 | -0.65 | 0.94 | — | -1.00 | 3.778 | 2.16 |
| NGC6352 | L | 1.98 ± 0.05 | 1.33 ± 0.04 | 2.37 ± 0.03 | -0.70 | — | 0.0 | -1.00 | — | — |
| NGC6356 | L | 2.40 ± 0.04 | 1.58 ± 0.03 | 2.42 ± 0.02 | -0.50 | 0.97 | 0.0 | -1.00 | 3.756 | 1.12 |
| NGC6362 | L | 2.53 ± 0.06 | 1.99 ± 0.05 | 1.56 ± 0.03 | -0.95 | 0.92 | 55.1 | -0.58 | 3.954 | 1.47 |
| NGC6388 | H | 2.89 ± 0.02 | 1.86 ± 0.02 | 2.14 ± 0.02 | -0.60 | — | 2.4 | -0.70 ^g | 4.255 | 1.01 |
| NGC6441 | H | 2.91 ± 0.03 | 1.80 ± 0.02 | 2.38 ± 0.02 | -0.53 | — | 0.3 | -0.70 ^g | 4.230 | 1.10 |
| NGC6528 | H | 3.00 ± 0.04 | 1.59 ± 0.03 | 3.32 ± 0.02 | -0.04 | — | 0.0 | -1.00 | — | — |
| NGC6553 | H | 2.94 ± 0.05 | 1.52 ± 0.04 | 3.25 ± 0.03 | -0.21 | — | 1.6 | -1.00 | — | — |
| NGC6569 | L | 2.53 ± 0.08 | 1.73 ± 0.07 | 1.79 ± 0.04 | -0.86 | — | 0.0 | — | 3.954 | 1.12 |
| NGC6624 | L | 2.55 ± 0.03 | 1.66 ± 0.02 | 2.23 ± 0.02 | -0.44 | 0.88 | 0.0 | -1.00 | 3.771 | 1.73 |
| NGC6637 | L | 2.35 ± 0.03 | 1.55 ± 0.03 | 2.11 ± 0.02 | -0.70 | 0.91 | 0.0 | -1.00 | 3.748 | 1.41 |
| NGC6638 | L | 2.54 ± 0.05 | 1.77 ± 0.04 | 1.79 ± 0.03 | -0.99 | 0.87 | 18.3 | -0.30 | 4.097 | 1.14 |
| NGC6652 | H | 2.86 ± 0.03 | 2.03 ± 0.02 | 1.73 ± 0.02 | -0.96 | 0.92 | 0.0 | -1.00 | 4.000 | 2.14 |
| NGC6723 | L | 2.64 ± 0.05 | 2.13 ± 0.04 | 1.26 ± 0.03 | -1.12 | 0.97 | 20.5 | -0.08 | 4.130 | 1.05 |

^a GGCs with high (H) and low (L) $H\beta$ indices at fixed metallicity.

^b Measured at FWHM = 3.1 Å spectral resolution.

^c From the Harris (1996, February 2003 revision) catalogue.

^d Relative GGC ages from De Angeli et al. (2005) and Recio-Blanco et al. (2006).

^e Maximum T_{eff} along the HB, from Recio-Blanco et al. (2006).

^f $S_{\text{BSS}}^{r,c} = \log(N_{\text{BSS}}/L_{F555w})$ inside the core radius. L_{F555w} in units of $10^4 L_{\odot}$. Taken from Moretti et al. (2008).

^g NGC6388 value taken from Zoccali et al. (2000). The same value is assumed for NGC6441 (Puzia et al. 2002).

- Puzia, T. H., Saglia, R. P., Kissler-Patig, M., Maraston, C., Greggio, L., Renzini, A., & Ortolani, S. 2002, *A&A*, 395, 45
- Puzia, T. H., Kissler-Patig, M., Thomas, D., Maraston, C., Saglia, R. P., Bender, R., Goudfrooij, P., & Hempel, M., 2005, *A&A*, 439, 997
- Rich, R. M., Sosin, C., Djorgovski, S. G., Piotto, G., King, I. R., Renzini, A., Phinney, E. S., Dorman, B., Liebert, J., & Meylan, G. 1997, *ApJ*, 484, 25
- Recio-Blanco, A., Aparicio, A., Piotto, G., De Angeli, F., & Djorgovski, S. G. 2006, *A&A*, 452, 875
- Rose, J. A. 1985, *AJ*, 90, 1927
- Sánchez-Blázquez, P., Peletier, R. F., Jiménez-Vicente, J., Cardiel, N., Cenarro, A. J., Falcón-Barroso, J., Gorgas, J., Selam, S., & Vazdekis, A. 2006, *MNRAS*, 371, 703
- Sánchez-Blázquez, P., Gorgas, J., Cardiel, N., & González, J. J. 2006, *A&A*, 457, 809
- Sandage, A. R. 1953, *AJ*, 58, 61
- Schiavon, R. P., Faber S. M., Rose, J. A., & Castilho, B. V. 2002, *ApJ*, 580, 873
- Schiavon, R. P., Rose, J. A., Courteau, S., & MacArthur, L. A. 2004, *ApJ*, 608, 33
- Schiavon, R. P., Rose, J. A., Courteau, S., & MacArthur, L. A. 2005, *ApJS*, 160, 163 (S05)
- Trager, S. C., Faber, S. M., Worthey, G., & González, J. J. 2000, *AJ*, 120, 165
- Trager, S. C., Worthey, G., Faber, S. M., & Dressler, A. 2005, *MNRAS*, 362, 2
- Vazdekis, A., Salaris, M., Arimoto, N., & Rose, J. A. 2001, *ApJ*, 549, 274
- Vazdekis, A. 1999, *ApJ*, 513, 224
- Vazdekis, A., Cenarro, A. J., Gorgas, J., Cardiel, N., & Peletier, R. F. 2003, *MNRAS*, 340, 1317
- Worthey, G., Faber, S. M., González, J. J., & Burstein, D. 1994, *ApJS*, 94, 687
- Worthey, G., & Ottaviani, D. L. 1997, *ApJS*, 111, 377
- Zoccali, M., Cassisi, S., Bono, G., Piotto, G., Rich, R. M., & Djorgovski, S. G. 2000, *ApJ*, 538, 289

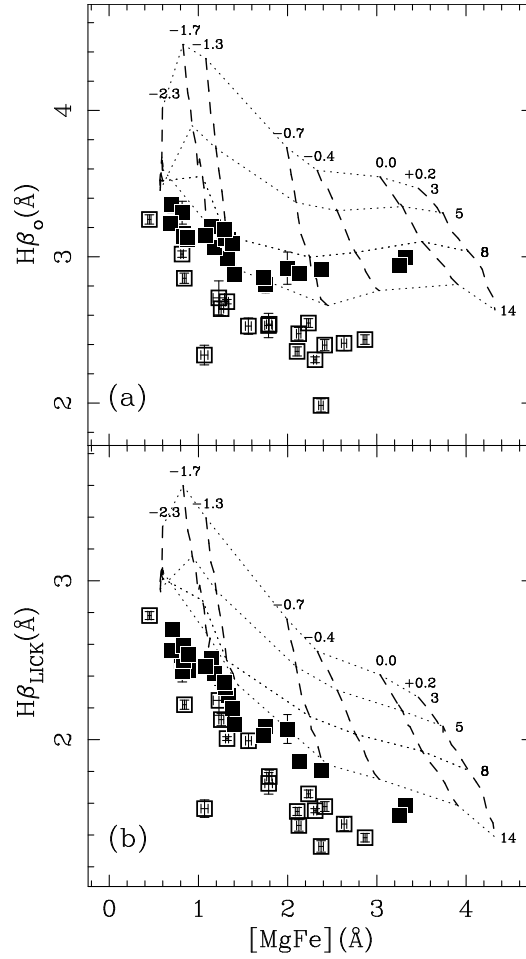


FIG. 1.— $H\beta_o$ (a) and $H\beta_{\text{LICK}}$ (b) indices versus $[\text{MgFe}]$ for the 41 GGCs in S05. Solid and open symbols indicate, respectively, GGCs with high (GGCH) and low (GGCL) $H\beta$ indices at fixed $[\text{MgFe}]$. SSP models from V99+ at $\text{FWHM} = 3.1\text{\AA}$ are overplotted, with dotted and dashed lines indicating fixed ages and metallicities as in the labels.

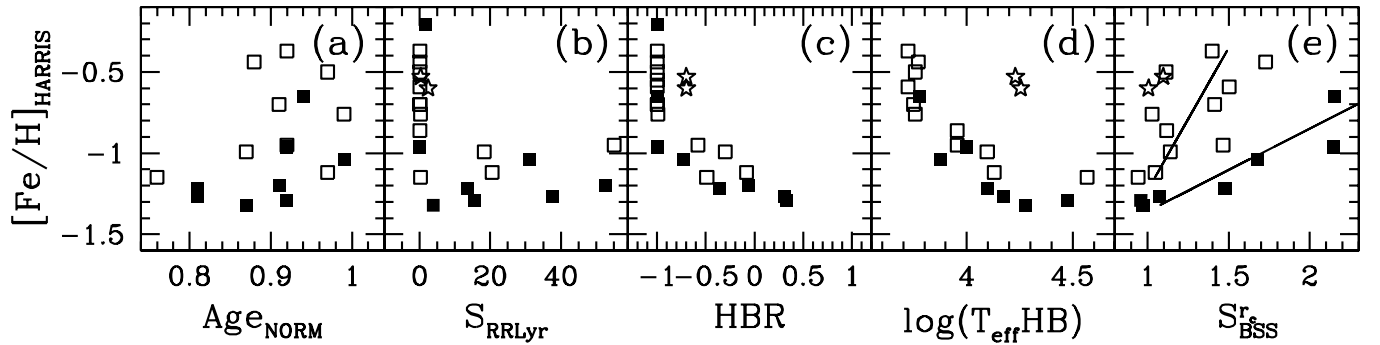


FIG. 2.— Metallicity versus CMD-derived parameters (Age_{NORM} , S_{RRLyr} , HBR, $\log(T_{\text{eff}} \text{HB})$, and S_{BSS}^r ; see definition in the text) for a subsample of 25 GGCs from S05 with $[\text{Fe}/\text{H}] > -1.35$. Symbol codes are kept as in Fig 1 except for the second parameter GGCs NGC6388 and NGC6441 (open stars). Solid lines in panel e illustrate individual linear fits to solid and open squares.